STUDIES ON SPECTRAL AND PHOTO LUMINESCENCE PROPERTIES OF Sm^{3+} IONS IN SODIUM LEAD ALUMINO BOROSILICATE GLASSES

[1] K. Vijaya Babu[*], [2] K. Naresh Kumar, [3] A. Subba Rao.
[1] Head of the Department of Physics, Bapatla College of Arts & Sciences, Bapatla.
[2] Lecturer in Physics, VRS & YRN College, Chirala.
[3] Lecturer in Physics, SS & N College, Narasaraopet.
[1] Department of Physics,
Bapatla College of Arts & Sciences, Bapatla. Andhra Pradesh, India.

Abstract: ***Sm_2O_3-doped Sodium lead alumino borosilicate (NPABS) glasses are prepared by the melt quenching technique and are characterized through various spectroscopic techniques such as X-ray diffraction spectra, the glassy nature of the present glass matrices are confirmed by XRD analysis. The Optical band gap and Urbach energies have been evaluated from the absorption edges of the absorption spectra of Sm_2O_3 doped prepared glasses. The Judd-Ofelt (JO) analysis has been applied to evaluate the intensity parameters, Ω_λ (λ=2, 4 and 6), experimental and theoretical oscillator strengths are also determined and reported. These JO parameters have been used to evaluate radiative properties such as radiative transition probabilities, branching ratios, radiative life time and stimulated emission cross-sections for the luminescent levels of Sm^{3+} ion. From the photoluminescence spectra the glasses shows the strongest emission at 601 nm when they are excited by 402 nm. The optimum concentration of Sm_2O_3 in titled glass is 1.0 mol% which exhibit the highest intensity of emission. The CIE color chromaticity coordinates have also been calculated to characterize the emission of the prepared glasses. The color purity and the correlated color temperature are also calculated and the results were discussed in the present work. The lifetime corresponding to the $^4G_{5/2}$ level of the title glasses has been found to decrease with the increase in Sm^{3+} ion concentration which may be causes luminescence quenching, energy transfer through cross-relaxation. The results indicate that the present glasses could be useful for photonics applications. Among the prepared glasses, NPABSSm10 glass exhibits higher β_R, σ_P^E, σ_P^E x τ_R, σ_P^E x $\Delta\lambda_{eff}$ values corresponding to the $^4G_{5/2} \rightarrow {}^6H_{7/2}$ emission band and these are in turn specifies its suitability for LEDs and visible laser applications.***

Keywords: Borosilicate glasses, Judd-Ofelt theory, Radiative properties, Photoluminescence spectra, Decay profile.

I. INTRODUCTION

Borosilicate glasses are used in a wide range of technological applications, from chemically resistant containers and piping to fiber composites, and from pharmaceutical, and sealing glasses to nuclear waste immobilization. The controlled heat treatment of borosilicate glasses especially those which have domain sizes in sub optical scale is interesting in controlling and designing the physical properties such as chemical durability, crystal nucleation rates, high-temperature strength, and is of interest in some natural magnetic systems as well. Due to these interesting physical properties, borosilicate glasses can be used as laser host matrices after doping with rare earth oxides [1-7]. Consequently, the structure of silicate groups formed on the amalgamation of SiO_2 in alkali borate glasses has been found to depend on the concentration and distribution of a variety of units containing BO_3 triangles, BO_4 tetrahedra that are bonded to a variety of cations of modifying oxides by non-bridging oxygens (NBOs) or by bridging oxygens (BO). Na_2O is a common flux, reduce the dispensation temperature and changes the properties of glass [8].The presence of Al_2O_3 in the glass matrix makes the glasses more resistant to attack by alkali metal ions like Li^+ and Na^+. This is clearly because of the entering of Al_2O_3 into the glass network with AlO_4 structural units that crosslink the neighboring borate and silicate chains [9]. Al_2O_3 is often used to modify the glass structure which improves chemical stability and physical properties. The Al^{3+} ions not only affect thermo-mechanical properties but also laser properties. Al_2O_3 mixed borosilicate glasses are being widely used in industrial applications as sealing materials, separators in batteries, microwave cavities, and dental cement components etc [10]. Higher NBOs contents generally lower the viscosity of the precursor glass melt but contribute to ease of corrosion; higher BO contents often lead to harder, more durable glasses that must be melted and worked at higher temperature based on different studies, it has been established that the mutual influence between the coordination types of Silicon in lead borosilicate glasses were attributed to two reasons. Among the glass components, Al_2O_3 has useful significant consideration as the most possible glass composition due to its high solubility of rare earth ions [9]. RE has a structure similar to that of Al_2O_3, in which RE ions have a preference for eight fold or nine- fold coordination. The charge of the RE ions is compensated by the oxygen's surrounding the Al^{3+} ions, which results in a homogeneous diffusion of the RE ions in the glass structure. Though, in the meantime, it is difficult to prepare a glass containing large amounts of Al_2O_3 because of its high melting temperature. PbO is one of the best glass modifiers which improve physical properties of glasses, since PbO is able to form stable glasses. PbO based glasses are widely used as the transparent dielectric layer of Plasma Display Panels [11].

Rare earth (RE) ions have been widely investigated in various host matrices due to their important roles in developing various optoelectronic devices such as optical sensors, phosphors, lasers, solar cell and optical amplifiers [12-17]. The elaboration of RE-based glasses for these applications requires an accurate knowledge of the radiative properties of RE ions in glasses. The Judd-Ofelt theory, developed to calculate the intensities of forced electric dipole transitions between 4f states, allows the phenomenological parameters related to the radiative properties of a particular glass composition to be determined [18].

Among Ln^{3+} ions, the trivalent samarium (Sm^{3+}) ion is one of the most interesting ions to analyze the fluorescence properties that exhibit strong orangish-red emission. Because of these reasons the glasses doped with Sm^{3+} ions find applications in color display systems, high dense information optical memory storage devices, submarine communication, solid state lasers in visible lasers needed for next generation nuclear fusion and gain media in the microchip laser at higher doping levels, and photodynamic therapy (PDT) light sources owing to its emitting $^4G_{5/2}$ level exhibiting relative high internal quantum and multi-fluorescence channels [18-23].

The present work reports the results obtained in the Sm^{3+} doped title glasses thoroughly studied by using the spectroscopic techniques such as absorption, photoluminescence and decay measurements. The Judd-Ofelt (JO) intensity parameters Ω_λ (λ = 2, 4, 6) determined from the measured oscillator strengths (f_{exp}) are used in evaluating the radiative properties such as spontaneous transition probabilities (A_R), total transition probabilities (A_T), radiative branching ratios (β_R) and radiative lifetimes (τ_R) for the observed fluorescent levels of Sm^{3+} ions in NPABS glasses. The laser characteristic parameters namely the experimental branching ratios (β_{exp}), stimulated emission cross-sections (σ_p^E), gain bandwidths (σ_p^E x $\Delta\lambda_{eff}$), optical gain (σ_p^E x τ_R) and quantum efficiency (η) are evaluated to optimize the doped rare earth ion concentration in title glasses for solid state lasers and optical fiber amplifiers in visible region.

2. EXPERIMENTAL

Sm^{3+} doped sodium lead alumino borosilicate glasses are prepared by conventional melt quenching technique using appropriate quantities (in mol %) of high-purity Na_2O, PbO, Al_2O_3, B_2O_3, SiO_2 and Sm_2O_3 powders according to the molar host composition 20 Na_2O-10 PbO-(5-x) Al_2O_3-40 B_2O_3-25 SiO_2. Additional 0.5 mol%, 1.0 mol% and 1.5 mol% Sm_2O_3 powders are doped into NPABS glass composition based on the host weight. First, the raw materials are well ground in an agate mortar and melted in an electric furnace at 1200^{o}C for 20 min. in a silica crucible. The melt is then air quenched by pouring it on a thick brass plate. The glass samples are annealed at 400^{o}C for 12h to remove residual strain and polished for optical measurements. The refractive indices of the samples are determined with an Abbes refractometer using monobromo naphthalene as an optical coating with an accuracy ±0.001 and the density measurements are carried out using Archimedes principle with O-xylene as an immersion liquid.

Optical absorption spectra of the polished samples are measured using JASCO UV-VIS-NIR spectrophotometer (model V-670) at room temperature (RT) in the range 200 - 2000 nm. The X-ray powder diffraction pattern of prepared glass samples are recorded using XRD-6100 SHIMADZU X-Ray diffract meter in the scanning range of 10 - 80^0 (2θ) using Cu K_α radiation having a wavelength of 1.5406 Å at room temperature. The Fourier transform infrared analysis is carried out by glass matrix with KBr using SHIMADZU-IRAffinity-1S FT-IR spectrophotometer in the region of 4000 - 400 cm^{-1}. The emission and excitation spectra for all the glasses are recorded at room temperature using Shimadzu RF-5301 PC-Spectrofluorophotometer with a spectral resolution 0.5 nm. The time-resolved photoluminescence (PL) measurements are carried out using home-built setups with 385.6 nm (CW laser) as the excitation source. The emission from sample is coupled into a monochromator (Acton SP2300) coupled to CCD (charge coupled detector) through the appropriate lenses and filters. For time-resolved photoluminescence, a frequency generator (5 Hz), lock-in amplifier, digital storage oscilloscope and a monochromator (Acton SP2300) coupled to a photomultiplier tube (PMT) are employed. The confocal photoluminescence images are recorded by using a modified laser scanning confocal microscope (Olympus, BX51) equipped with XYpiezo state and excited with 402 nm CW laser.

3. RESULTS AND DISCUSSION

3.1 Physical properties

Fig. 1 shows optically polished glasses for the measurement of physical parameters, such as density and refractive index. It is observed that with the addition of Sm_2O_3 content glasses becomes orange in color. From the experimentally measured densities and refractive indices different physical properties of titled glasses evaluated, are presented in **Table 1**. Density is an effective tool to investigate the degree of structural compactness, modifications of geometrical configurations of the glass network, change in co-ordination and the variation of dimensions of interstitial holes [24]. Refractive index is one more important parameter for the optical materials. From **Table 1**, it can be found that, the density and molar volume of the glasses increase with increase in Sm^{3+} ion concentration. The higher molecular weight of Sm_2O_3 than other oxides also has significant effect on increase in density of glasses with Sm_2O_3. The increasing nature of molar volume with Sm_2O_3 reveals that addition of Sm_2O_3 opens the glass structure. Increase in molar volume with the addition of Sm_2O_3 may be due to the greater ionic radius of Sm^{3+} as compared to other glass constituents. [25]. **Fig. 2** shows the variation of density and molar volume with the addition of Sm_2O_3.

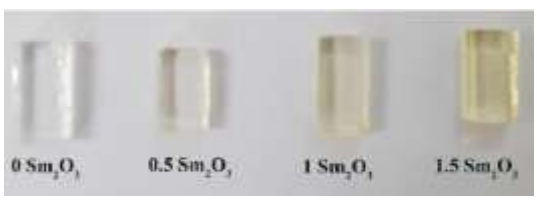

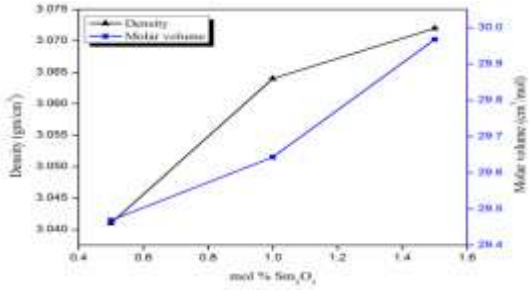

Fig. 1 Glasses with different concentrations of Sm^{3+} ion doped NPABS glasses

Fig. 2 The variation of density and molar volume with the addition of Sm_2O_3

Table 1 Physical properties of the Sm^{3+} doped sodium lead alumino borosilicate glasses

Parameters	Sample code			
	Pure	NPABSSm5	NPABSSm10	NPABSSm15
Density (ρ) g/cm^3	2.960	3.041	3.064	3.072
Molar volume (V_m) cm^3/mol	29.854	29.469	29.643	29.967
Dysprosium ion con. (N_i)x10^{20}	-	1.022	2.032	3.015
Inter ion separation (r_i) Å	-	21.389	17.01	14.914
Polaran radius (r_p) Å	-	8.618	6.854	6.009
Refractive index (n_d)	1.653	1.654	1.655	1.657

3.2 X-ray diffraction analysis

Fig. 3 shows the X-ray diffraction pattern of Sm^{3+} doped glasses recorded in the range $5^0 \leq \theta \leq 80^0$. The spectrum exhibited broad diffused scattering at low angles, which is the characteristic long range structural disorder that confirms the amorphous nature [26].

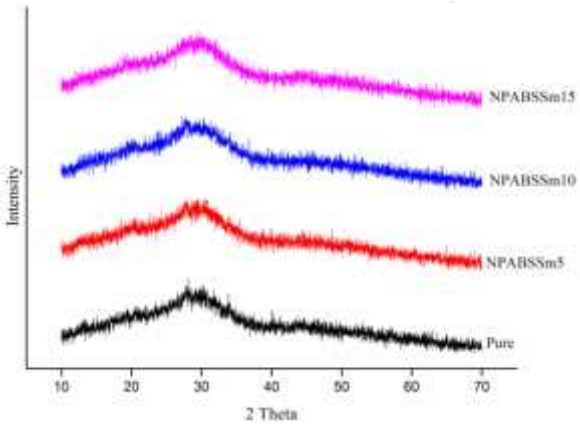

Fig. 3 XRD pattern of NPABSSm glasses

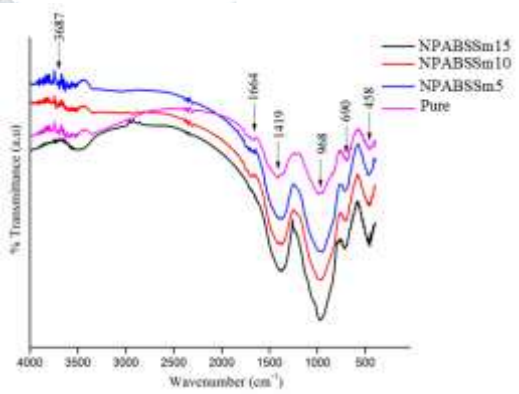

Fig. 4 FTIR spectra of Sm^{3+} doped NPABS glasses

3.3 Fourier Transform Infrared spectral analysis

Fourier transform infrared spectra (FT-IR) of the glasses are recorded in transmittance mode at room temperature. **Fig. 4** represents the FT-IR spectra of the undoped and title glasses with varying concentration of Sm^{3+} ions. The broad absorption peak in the wavenumber region 3200-3700 cm^{-1} belongs to the hydroxyl group due to OH stretching vibrations. The broad absorption peak between the wavenumber 1200 and 1500 cm^{-1} is due to the asymmetric stretching relaxation of B-O bonds from the BO_3 trigonal units. The B-O bond stretching of BO_4 tetrahedral units gives the peak within the range 800-900 cm^{-1}. The peak between 600 and 750 cm^{-1} represents various B-O-B bending modes in BO_3 and BO_4 units [27-29] in the prepared glasses are presented in **Table 2.**

Table 2 The observed FTIR band positions (cm^{-1}) and their assignment of the Sm^{3+} doped sodium lead alumino borosilicate glasses

S. No	Sample code				Assignment
	Pure	NPABSSm5	NPABSSm10	NPABSSm15	
1	454	462	462	458	Characteristic vibration of cation-oxygen SiO_4, BO_4, AlO_6 tetrahedral groups
2	707	704	704	690	B-O-B bending modes in BO_3, BO_4 and AlO_4 units
3	960	960	961	968	Symmetric stretching vibrations of Si-O-Si bonds in SiO_4 tetrahedral units
4	1376	1387	1380	1419	Asymmetric stretching vibrations of [BO_3] units. [BO_3] convert to [BO_4]
5	1688	1688	1681	1664	Stretching vibrations of borate triangles.
6	3592	3682	3682	3687	Hydroxyl groups

3.4 Optical absorption spectra and nephelauxetic effect

Fig. 5 shows UV-Vis-NIR spectra of the prepared glasses recorded at room temperature in the wavelength region 350-1800 nm. The absorption bands of the present glasses are found to be alike and exhibit small differences in their intensities. Each spectrum exhibit twenty absorption bands due to the 4f-4f transition of the Sm^{3+} ions from the $^6H_{5/2}$ ground state to the various excited energy levels such as $^4D_{3/2}$, $^6P_{7/2}$, $^4L_{15/2}$, $^6P_{3/2}$, $^4M_{19/2}$,$^6P_{5/2}$, $^4G_{9/2}$, $^4F_{5/2}$, $^4I_{13/2}$, $^4M_{15/2}$, $^4I_{9/2}$, $^4G_{7/2}$, $^4F_{3/2}$, $^6F_{11/2}$, $^6F_{9/2}$, $^6F_{7/2}$, $^6F_{5/2}$, $^6F_{3/2}$, $^6H_{15/2}$ and $^6F_{1/2}$ centered at 361, 373, 390, 403, 417, 420, 433, 438, 462, 469, 488, 500, 524, 940, 1072, 1221, 1366, 1469, 1524 and 1583 nm respectively [30-32]. The absorption band assignments, the corresponding band positions of the prepared glasses are presented in **Table 3** along with that of the aquo-ion. From the absorption spectra it is observed that, the intensity of the bands in the NIR region are found to be more intense compared to the bands in the UV-Vis region, because of the fact that the transitions from the $^6H_{5/2}$ ground state to the excited states such as ^6F_J (J =11/2, 9/2, 7/2, 5/2, 3/2 and 1/2) and $^6H_{15/2}$ are spin allowed $|\Delta S| = 0$ [33]. Among the observed transitions, $^6H_{5/2} \rightarrow {}^6F_{1/2}$ and $^6F_{3/2}$ transitions are hypersensitive in nature which obey the selection rules $|\Delta S| = 0$, $|\Delta L| \leq 2$ and $|\Delta J| \leq 2$ and are sensitive to the ligand field environment around the RE ion site. Due to the overlapping of 4f electronic orbitals of the RE ions with the oxygen orbitals caused by the Nephelauxetic effect the RE ions exhibit shift in their energy level positions when doped into the glass matrices. This change in RE ion energy level positions gives an idea about the nature of the bonding between oxygen and RE-ligand. The metal-ligand bonding nature has been evaluated from the Nephelauxetic ratios (β) and bonding parameter (δ) studies. The Nephelauxetic ratio ($\beta = \upsilon_c/\upsilon_a$) is defined as the ratio of wave number of a particular RE ion transition (υ_c) to the corresponding aquo-ion transition (υ_a). The δ values can be calculated using the below given expression [32, 26],

$$\delta = \frac{1-\bar{\beta}}{\bar{\beta}} \times 100 \qquad (1)$$

where $\bar{\beta}$ is the average value of the Nephelauxetic ratio (β). The calculated $\bar{\beta}$ and δ values of the studied glasses are presented in **Table 3** and the negative sign of the δ values specify the ionic nature of the Sm-O bond in the title glasses. Generally, interactions of network former with the surrounding oxygen ions determine the strength of the covalence between RE^{3+}-O. Due to the difference in electro negativity of the two network formers, the interaction of silicate ions with the surrounding oxygen is stronger compared to the boron and it controls the polarization of oxygen upon Sm^{3+} ions. The addition of Sm_2O_3 content into the glass matrix causes only a slight deviation in the energy level positions of the Sm^{3+} ions which has been observed from the average Nephelauxetic ratio values that exhibit minor changes and is presented in **Table 3**.

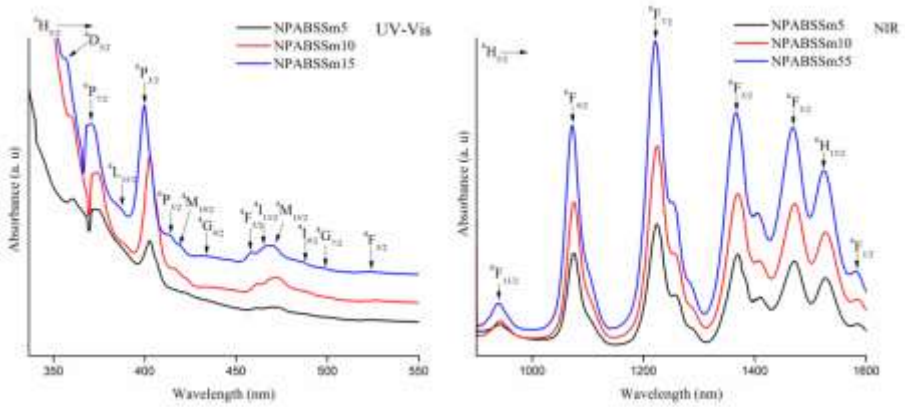

Fig. 5 Absorption spectra of NPABSSm glasses in UV-Vis and NIR regions

Table 3 The energy level positions (cm^{-1}) and bonding parameters ($\bar{\beta}$, δ) of the Sm^{3+} doped sodium lead alumino borosilicate glasses

Transitions	Sample code			Aquo-ion
	NPABSSm5	NPABSSm10	NPABSSm15	
$^4D_{3/2}$	27716	27777	27700	27700
$^6P_{7/2}$	26831	26737	26809	26750
$^4L_{15/2}$	25713	25706	25641	25676
$^6P_{3/2}+{}^4F_{7/2}$	24820	24813	24813	24950
$^4M_{19/2}$	23674	23646	23809	24164
$^6P_{5/2}$	23980	23992	23980	24069
$^4G_{9/2}$	23094	23041	23094	22795
$^4F_{5/2}+{}^4M_{17/2}$	21691	21654	22831	22700
$^4I_{13/2}$	21739	21321	21645	21100
$^4M_{15/2}$	21119	21119	21321	20753
$^4I_{9/2}$	20374	20374	20491	20536
$^4G_{7/2}$	19960	19960	20008	20024
$^4F_{3/2}$	18989	18989	19083	18921
$^6F_{11/2}$	10621	10621	10643	10500
$^6F_{9/2}$	9311	9302	9325	9200
$^6F_{7/2}$	8169	8163	8190	8000
$^6F_{5/2}$	7299	7299	7320	7100
$^6F_{3/2}$	6798	6798	6807	6630
$^6H_{15/2}$	6553	6553	6561	6565
$^6F_{1/2}$	6301	6309	6317	6400

$\bar{\beta}$	1.0062	1.00735	1.00693
δ	-0.616	-0.730	-0.688

3.5 Optical band gap and Urbach's energy analysis

The optical band gap energy (E_{opt}) is an important parameter for describing solid-state materials. The study of the fundamental absorption edge in the UV -region is a useful method for the investigation of optical transitions and electronic band structure in crystalline and amorphous materials. There are two types of optical transitions, which can occur at the fundamental absorption edge of crystalline and amorphous material. They are direct and indirect transitions. In both the cases, electromagnetic waves interact with the electrons in the valance band, which are raised across the fundamental gap to the conduction band. In glasses the conduction band is influenced by the glass forming anions, the cations play an indirect but are important role [34]. The absorption coefficient α(ν) is calculated from the absorbance (A) using the following equation:

$$\alpha(\nu) = \left(\frac{1}{d}\right) \ln\left(\frac{I_0}{I}\right) = 2.303 \left(\frac{A}{d}\right) \quad (2)$$

where A is the absorbance at frequency ν and d is the thickness of the sample. For an absorption by an indirect transition, the equation takes the form:

$$\alpha h\nu = B(h\nu - E_{opt})^n \quad (3)$$

where B is a constant and hν is the photon energy, E_{opt} is the optical energy gap and n is an index. The values of n are 1/2 and 2 for direct and indirect transitions, respectively. Using the above Eq. (3), by plotting $(\alpha h\nu)^2$ and $(\alpha h\nu)^{1/2}$ as a function of photon energy hν. The Tauc's plots of the prepared glasses are shown in **Fig. 6**. The direct band gap values are found to be 4.043 eV, 4.017 eV, 3.991 eV and 3.939 eV corresponding to the Pure, NPABSSm5, NPABSSm10 and NPABSSm15 glasses respectively. The indirect band gap values vary from 3.9756 to 3.9713 eV following the same trend as that of the direct band gap values and the results are presented in **Table 4**. It is observed from the table that while introducing the Sm^{3+} ions into the host matrix the direct and indirect band gap values are found to decrease with increase in Sm_2O_3 content. This indicates the fact that the wavelengths of the optical absorption edge of the prepared glasses shift towards the lower energy side of the electromagnetic spectrum due to the formation of more number of NBOs created in the host matrix by the structural rearrangement of BO_3 units into BO_4 units because of the fact that NBOs binds excited electrons less tightly than the bridging oxygen [33]. Urbach's energy relates to the optical transition between the tail end of the valance band and the conduction band which is extended into the band gap and is used to characterize the degree of disorderness of the amorphous materials. The Urbach's energy (ΔE) values are found to vary between 0.2637 eV to 0.2795 eV [31]. It is observed from **Table 4** that the band gap and the Urbach's energy values follow the opposite trend i.e. when the band gap values decreases the Urbach's energy values are found to increase due to the Sm^{3+} ions content in the prepared glasses which may delocalize some of the localized states present in the energy levels through the structural rearrangement in the glass network.

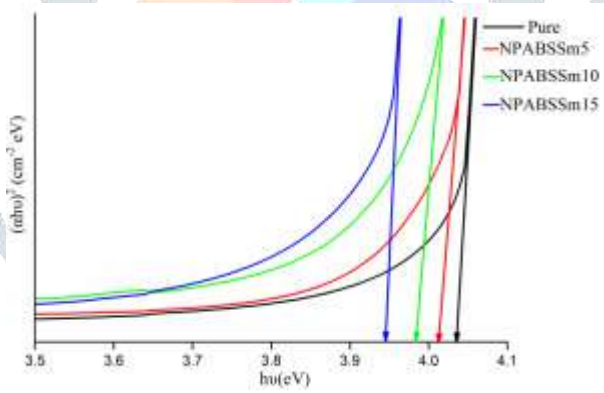

Fig. 6 Tauc's plot of the Sm^{3+} doped NPABS glasses

Table 4 The fundamental absorption edge (λ_{edge}), Optical band gap (E_{opt}) and Urbach energy (ΔE) corresponding to n = 1/2 and 2 for the Sm^{3+} ions doped sodium lead alumino borosilicate glasses

Sample code	λ_{edge} nm	Energy band gap (E_{opt}) (eV)			Urbach energy (ΔE)
		Calculated	Direct	Indirect	
Pure	305	4.066	4.043	3.971	0.2637
NPABSSm5	306.5	4.053	4.017	3.935	0.2708
NPABSSm10	307	4.046	3.991	3.891	0.2746
NPABSSm15	312.5	3.975	3.939	3.823	0.2795

3. 6 Oscillator strength and Judd-Ofelt analysis

The energies of an absorption transitions originating from the ground state of RE ions in a host matrix can be expressed in terms of oscillator strengths. Such experimental oscillator strengths can be measured by taking the integrated areas under the absorption peaks of the absorption spectrum by using the following expression [32].

$$f_{exp} = \frac{2.303mc^2}{N\pi e^2} \int \varepsilon(\upsilon)d\upsilon = 4.318 \times 10^{-9} \int \varepsilon(\upsilon)d\upsilon \quad (4)$$

where m and e are mass and charge of an electron, c is the velocity of light, N is the Avogadro's number and $\varepsilon(\upsilon)$ is the molar absorptivity of a band at a wave number υ (cm^{-1}).

By applying the J-O theory the calculated oscillator strengths f_{cal} of an electric dipole transition from an initial state (ψJ) to an excited state ($\psi' J'$) within the 4f configuration can be obtained using JO theory from the following expression [32],

$$f_{cal} = \left[\frac{8\pi^2 mc\theta}{3h(2j+1)}\right]\left[\frac{(n^2+2)^2}{9n}\right] x \sum_{\lambda=2,4,6} \Omega_\lambda (\varphi J \| U^\lambda \| \varphi' J')^2 \quad (5)$$

By using the experimental spectral intensities and the reduced square matrix elements, Ω_λ (2, 4 and 6) are the J-O intensity parameters and $\|U^2\|^2$, $\|U^4\|^2$ and $\|U^6\|^2$ are the doubly reduced square matrix elements and their values are chosen from the reported literature [25]. The J-O intensity parameters are obtained from the absorption spectra by taking the least square fitting approximation between the experimental and calculated oscillator strengths [26, 24]. The f_{exp} and f_{cal} values along with the root mean square (δ_{rms}) deviation values are presented in **Table 5**. The lower δ_{rms} values indicate the quality of the fit between f_{exp} and f_{cal} values and the validity of the Judd-Ofelt theory. Once the values of Ω_λ are obtained, the other radiative parameters such as electric dipole line strength (S_{ed}), magnetic dipole line strength (S_{md}), spontaneous transition probabilities (A_R), total transition probability (A_T), radiative lifetime (τ_{rad}) and branching ratios (β_R) corresponding to different emission channels from $^4G_{5/2}$ level are calculated [35] and presented in **Table 6**.The Ω_2 intensity parameter is mainly affected by the asymmetry of the ligand field environment around the RE^{3+} ions as well as the covalency of the RE-O bond. The Ω_4 and Ω_6 parameters are related to the bulk properties such as viscosity and rigidity of the RE-O bond in the RE^{3+} doped glasses [27]. J-O intensity parameters are found to be in the order of $\Omega_2 < \Omega_4 < \Omega_6$ for the Sm^{3+}: NPABS glass and presented in **Table 7**. The information related to the structural changes and symmetry environment of the ligand field and covalency could be deduced from the intensity parameter Ω_2. For the present glass Ω_2 was small, which suggests the ionic nature or low covalency of Sm-O bond under more Centro-symmetric or lower asymmetric environment around Sm^{3+} ions. The higher values of Ω_6 parameter indicate the high rigidity and viscosity of the host glass medium around the Sm^{3+} ions [36]. The J-O parameter values suggest the symmetry of the site occupied by the Sm^{3+} ions in the prepared glasses. The spectroscopic quality factor (Ω_4 / Ω_6) is estimated to be <1, this observation reveals that these glasses are used to describe the optical quality and is suitable for photonic applications of the prepared glasses compared to the other Sm^{3+} doped glasses [37-42] which are presented in the **Table 7**.

Table 5 Experimental and calculated oscillator strengths (x10 $^{-6}$), Number of transition and rms deviation (δ) of the Sm^{3+} doped sodium lead alumino borosilicate glasses

Transition from $^6H_{5/2} \rightarrow$	Barycenter (cm^{-1})	NPABSSm5		NPABSSm10		NPABSSm15	
		f_{exp}	f_{cal}	f_{exp}	f_{cal}	f_{exp}	f_{cal}
$^4D_{5/2}$	27700	0.501	0.593	0.714	0.758	0.609	0.601
$^6P_{7/2}$	26738	1.66	1.636	1.27	1.67	2.031	1.665
$^6P_{3/2}+^4F_{7/2}$	24876	3.007	3.896	3.83	3.21	3.319	3.041
$^6P_{5/2}+^4M_{19/2}$	24038	0.204	0.257	0.258	0.212	0.119	0.118
$^4F_{5/2}+^4M_{17/2}$	22831	0.446	0.473	0.445	0.588	0.327	0.447
$^4M_{15/2}+^4I_{9/2+11/2+13/2}$	21692	0.033	0.051	0.038	0.036	0.039	0.038
$^6F_{11/2}$	10615	0.446	0.835	0.423	0.538	0.399	0.447
$^6F_{9/2}$	9328	2.711	2.498	3.31	3.24	3.054	2.712
$^6F_{7/2}$	8176	3.685	3.546	4.32	4.36	4.257	3.692
$^6F_{5/2}$	7358	1.502	1.344	1.77	1.73	1.936	1.507
$^6F_{3/2}$	6557	0.685	0.6	0.732	0.789	0.695	0.685
$^6H_{15/2}$	6548	0.022	0.023	0.02	0.028	0.022	0.027
$^6F_{1/2}$	6301	0.026	0.029	0.039	0.034	0.057	0. 045
N		13		13		13	
δ_{rms} (x10^{-6})			± 0.283		± 0.214		± 0.255

Table 6 Electric (S_{ed} x10^{-23} cm^{-1}), magnetic (S_{md} x10^{-23} cm^{-1}) dipole line strengths, electric (A_{ed} s^{-1}), magnetic (A_{md} s^{-1}) radiative transition probabilities, total line radiative transition probabilities (A_R), total radiative transition probabilities (A_T, s^{-1}), luminescence branching ratios (β_R) and radiative lifetime (τ_{rad} μs) of the $^4G_{5/2}$ state of Sm^{3+} ions in NPABSSm10 glass

Transition	S_{md}	S_{ed}	A_{ed}	A_{md}	A_R	β_R
$^6F_{11/2}$	0.00	1.75	0.22	0	0.22	0.0005
$^6F_{9/2}$	0.00	1.51	0.21	0	0.21	0.0004

$^6F_{7/2}$	2.67	5.10	0.79	0.45	1.25	0.0029
$^6F_{5/2}$	6.62	4.97	0.96	1.41	2.37	0.0055
$^6F_{3/2}$	8.46	0.34	0.09	2.51	2.61	0.0060
$^6H_{15/2}$	0	0.59	0.23	0	0.23	0.0005
$^6F_{1/2}$	0	0.65	0.04	0	0.04	0.0001
$^6H_{13/2}$	0	5.89	6.33	0	6.3348	0.0146
$^6H_{11/2}$	0	20.3	48.54	0	48.54	0.1123
$^6H_{9/2}$	0	24.4	98.05	0	98.05	0.2268
$^6H_{7/2}$	5.81	49.3	233.98	14.57	248.55	0.5751
$^6H_{5/2}$	5.73	1.61	6.01	17.39	23.4	0.0541

$A_T = 432.18$; $\tau_{rad} = 2313$ μs

Table 7 Judd–Ofelt intensity parameters ($\Omega_\lambda \times 10^{-20}$ cm^2), spectroscopic quality factor (Ω_4 / Ω_6) in sodium lead alumino borosilicate glasses doped with Sm^{3+} ions

Sample code	J-O intensity parameters			Ω_4 / Ω_6	Trends of Ω_λ	Reference s
	Ω_2	Ω_4	Ω_6			
NPABSSm5	0.068	2.685	2.974	0.902	$\Omega_6 > \Omega_4 > \Omega_2$	[Present]
NPABSSm10	0.01	3.051	3.551	0.859	$\Omega_6 > \Omega_4 > \Omega_2$	[Present]
NPABSSm15	0.0151	3.323	3.354	0.990	$\Omega_6 > \Omega_4 > \Omega_2$	[Present]
ZnAlBiBSm20	0.021	2.55	4.18	-	$\Omega_6 > \Omega_4 > \Omega_2$	[37]
Glass D	0.067	3.162	4.610	0.686	$\Omega_6 > \Omega_4 > \Omega_2$	[38]
LBMBPS1	0.354	3.91	4.74	0.82	$\Omega_6 > \Omega_4 > \Omega_2$	[39]
LCM Borate	0.84	4.00	5.02	0.80	$\Omega_6 > \Omega_4 > \Omega_2$	[40]
CdBiB	0.040	2.84	6.03	-	$\Omega_6 > \Omega_4 > \Omega_2$	[41]
LSG8	0.627	4.858	5.335	-	$\Omega_6 > \Omega_4 > \Omega_2$	[42]

3. 7 Fluorescence spectra

The excitation spectra of the prepared glasses have been recorded in the wavelength region 325-500 nm monitoring an excitation wavelength at 601 nm and as a representative case excitation spectrum of the NPABSSm10 glass is shown in **Fig. 7**. The excitation spectra exhibit seven excitation bands at around 343, 360, 373, 402, 415, 435, and 468 nm corresponding to the transitions $^6H_{5/2} \rightarrow {}^4H_{9/2}$, $^6H_{5/2} \rightarrow {}^4D_{3/2}$, $^6H_{5/2} \rightarrow {}^4P_{7/2}$, $^6H_{5/2} \rightarrow {}^4F_{7/2}$, $^6H_{5/2} \rightarrow {}^6P_{5/2}$, $^6H_{5/2} \rightarrow {}^4G_{9/2}$ and $^6H_{5/2} \rightarrow {}^4H_{11/2}$ respectively [43], which are attributed to the f-f forbidden transitions of Sm^{3+} observed within the wavelength region of 300 nm to 500 nm (i.e., low energy). Among these, the band corresponding to the transition $^6H_{5/2} \rightarrow {}^4F_{7/2}$ (402 nm) is found to be more intense, and the same was used as an excitation wavelength to the recorded emission spectra of the title glasses. This finding also indicates that the prepared phosphor can be efficiently excited by UV (~400 nm) LED chips [27].

The fluorescence spectra of the present glasses have been recorded in the wavelength region 500-750 nm and are shown in **Fig. 8**. The title glasses emit bright reddish-orange luminescence from the $^4G_{5/2}$ initial state to the low lying levels $^6H_{J'}$ with J' = 5/2, 7/2, 9/2 and 11/2 respectively [44]. When any other energy transitions above the $^4G_{5/2}$ level are excited, there is an abrupt non-radiative relaxation to this excited fluorescent level. In the present observation, more intense emission bands at 564 nm, 600 nm, 648 nm and one feeble emission peak at 711 nm are observed and these emission peaks are assigned to the $^4G_{5/2} \rightarrow {}^6H_{5/2}$ (green), $^4G_{5/2} \rightarrow {}^6H_{7/2}$ (orange), $^4G_{5/2} \rightarrow {}^6H_{9/2}$ (red) and $^4G_{5/2} \rightarrow {}^6H_{11/2}$ (deep red) transitions, respectively. Among these, the emission bands corresponding to $^4G_{5/2} \rightarrow {}^6H_{7/2}$ $^4G_{5/2} \rightarrow {}^6H_{9/2}$ and $^4G_{5/2} \rightarrow {}^6H_{11/2}$ transitions exhibited intense luminescence emission, while the other two bands related to $^4G_{5/2} \rightarrow {}^6H_{5/2}$ and $^4G_{5/2} \rightarrow {}^6H_{11/2}$ transitions exhibited moderate intensity [37]. Notably, the $^4G_{5/2} \rightarrow {}^6H_{7/2}$ (600 nm) transition has the strongest intensity and can be applied to orange-red emitting display materials. Further the intensity of emission bands is found to increase with increasing of Sm^{3+} ion concentration up to 1.0 mol% and for higher concentrations (> 1.0mol%) it decreases. The quenching for higher concentrations of Sm^{3+} ion beyond 1.0 mol% could be of clustering of Sm^{3+} ion. Such effects give rise to the quenching of luminescence emission. In addition, the non-radiative transitions due to multi phonon relaxation, resonance energy transfer and cross relaxation channels also contribute to the luminescence quenching at higher concentrations of Sm^{3+} ions. However, the large energy gap between the excited level and the next lower energy level minimizes the multi phonon relaxation. Further, the energy of the transition $^4G_{5/2} \rightarrow {}^6F_{11/2}$ (7165 cm^{-1}) is nearly equal to that of the $^6H_{5/2} \rightarrow {}^6F_{5/2}$ transition (7179 cm^{-1}) and also the energy of $^4G_{5/2} \rightarrow {}^6F_{5/2}$ (10211cm^{-1}) transition matches with that of the transition $^6H_{5/2} \rightarrow {}^6F_{11/2}$ (10377 cm^{-1}) and hence luminescence quenching is subjected by the cross-relaxation channels in which the energy transfers between the intermediate energy levels as depicted (CR1 and CR2) in the partial energy level diagram shown in **Fig. 9**. The variation in luminescence intensity corresponding to the $^4G_{5/2} \rightarrow {}^6H_{7/2}$ transition and the orange/red intensity ratio with varying Sm^{3+} ion concentration in the prepared glasses have been presented in **Fig. 8**. The results show that the O/R ratio (orange to red band) is found to be 1.8977, 2.0947 and 1.8798 corresponding to the NPABSSm5, NPABSSm10 and NPABSSm15 glasses, respectively [47]. The luminescence intensity ratio (O/R) is found to be highest for 1.0 wt % Sm^{3+} ion doped glass and beyond that the ratio decreases owing to the concentration quenching created by the interaction between the Sm^{3+}- Sm^{3+} ions. The emission of Sm^{3+} ion in orange and red regions can be useful in developing powerful solid state lasers and also the emission in different regions encouraging the glasses to use in colour display systems.

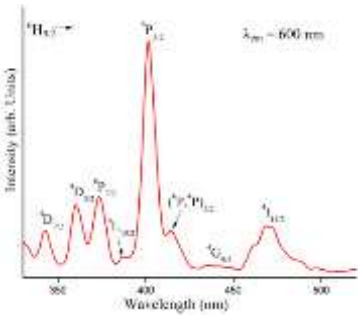

Fig.7 Excitation spectrum of the NPABSSm10 glass

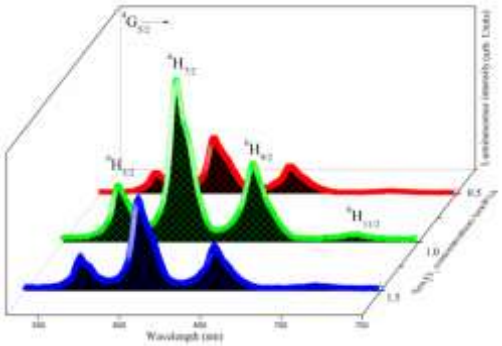

Fig.8 Luminescence spectra of the Sm^{3+} doped NPABS glasses

3.8 Radiative properties

The radiative transition probability (A_R) for a transition $\Psi J \rightarrow \Psi' J'$ can be calculated from the following equation

$$A_R(\Psi J, \Psi' J') = \left[\frac{64\pi^4\vartheta^3}{3h(2j+1)}\right]\left[\frac{n(n^2+2)^2}{9}S_{ed} + n^3 S_{md}\right] \quad (6)$$

where S_{ed} and S_{md} are the electric and magnetic-dipole line strengths respectively, calculated from the following expressions

$$S_{ed} = e^2 \sum_{\lambda=2,4,6} \Omega_\lambda (\varphi J \| U^\lambda \| \varphi' J')^2 \quad (7)$$

$$S_{md} = \frac{e^2h^2}{16\pi^2m^2c^2}\Omega_\lambda (\varphi J \| L + 2S \| \varphi' J')^2 \quad (8)$$

where $\|U^\lambda\|^2$ are the doubly reduced matrix elements of the unit tensor operator of rank λ = 2, 4 and 6 calculated from the intermediate coupling scheme and the Ω_λ are the host dependent J-O parameters. In J-O analysis, the reduced matrix elements and the S_{md} values are utilized from the reports by Jayasankar and Rukmini [43], since these matrix elements and S_{md} depend only on the RE ion but not on the host material. The S_{md} values also can be calculated using the formulae:

The radiative lifetime (τ_R) of an excited state is given by

$$\tau_R(\varphi J) = [A_T(\varphi J)]^{-1} \quad (9)$$

The branching ratio (β_R) corresponding to the emission from an excited $\varphi' J'$ level to its lower level φJ is given by,

$$\beta_R(\varphi J, \varphi' J') = \frac{A(\varphi J, \varphi' J')}{A_T((\varphi J)} \quad (10)$$

The branching ratios can be used to predict the relative intensities of all emission lines originating from a given excited state. The experimental branching ratios can be found from the relative areas of the emission bands.

The peak stimulated emission cross-section, $\sigma(\lambda_p)$ (φJ, $\varphi' J'$), between the emission levels ΨJ and $\Psi' J'$ having a probability of A (φJ, $\varphi' J'$) can be expressed as

$$\sigma(\lambda_p) = \frac{\lambda_p^4}{8\pi c n^2 \Delta\lambda_{eff}} A(\varphi J, \varphi' J') \quad (11)$$

where λ_p the transition peak wavelength and $\Delta\lambda_p$ is its effective line width found by dividing the area of the emission band by its average height.

The calculated radiative properties of the prepared glasses are presented in **Table 8**. The branching ratios (β_R) and stimulated emission cross-section (σ_p^E) values are important parameters for laser applications. The branching ratio (β_R) values are found to be higher for the $^4G_{5/2} \rightarrow {}^6H_{7/2}$ emission and β_R values follow the trend as $^4G_{5/2} \rightarrow {}^6H_{7/2} > {}^6H_{9/2} > {}^6H_{11/2} > {}^6H_{5/2}$ uniformly for all the prepared glasses. It is observed from **Table 8** that, the experimental branching ratio values having good agreement with theoretically values using Judd-Ofelt theory. The higher branching ratio values for the orange (601 nm) emission indicate its potential for laser applications [19].The stimulated emission cross-section (σ_p^E) indicates the rate of energy extraction by the external stimuli from the optical material and is directly proportional to the transition probability (A) and inversely proportional to the effective band width ($\Delta\lambda_{eff}$) of all the observed emission bands, $^4G_{5/2} \rightarrow {}^6H_{7/2}$ transition exhibit higher stimulated emission cross-section values (σ_p^E x10^{-22}) and are found to be 5.36, 10.832 and 5.015 corresponding to the NPABSSm5, NPABSSm10 and NPABSSm15 glasses and the peak stimulated emission cross section (σ_p^E) values follow the trend as $^4G_{5/2} \rightarrow {}^6H_{7/2} > {}^6H_{9/2} > {}^6H_{11/2} > {}^6H_{5/2}$ for the prepared glasses [48-50]. The higher stimulated emission cross-section value is an attractive feature for low threshold, high gain laser applications which are used to obtain continuous wave (CW) laser action. Among all the prepared glasses, NPABSSm10 exhibit higher stimulated emission cross section and branching ratio values for the $^4G_{5/2} \rightarrow {}^6H_{7/2}$ transition and is more suitable for potential laser applications in the intense reddish-orange emission at 600 nm which is highly useful in submarine communications and medical diagnostic applications [51].

chromaticity coordinates

In order to explore the emission color of the present Sm^{3+} doped glasses, emission spectra are characterized using CIE 1931 chromaticity diagram. Using this diagram, the composition of any color can be illustrated in terms of three primary colors such as blue, green and red. The spectral color can be obtained by adding three artificial colors called tristimulus values (X, Y and Z). The chromaticity coordinates (x, y, z) are calculated by taking the ratios of the X, Y, Z of the emission light to the sum of three tristimulus values [52]. In general, color chromaticity coordinates (x, y, z) are calculated using the below given expressions

$$x = \frac{X}{X+Y+Z} \quad (12)$$

$$y = \frac{Y}{X+Y+Z} \quad (13)$$

$$z = \frac{Z}{X+Y+Z} \quad (14)$$

The standard x, y coordinates (x= 0.33 and y = 0.33) corresponding to the location of the white light emission is always situated at the center of the CIE 1931 chromaticity diagram. The (x, y) values of the prepared glasses are calculated from the emission spectra and the values are found to be (0.5789, 0.4302), (0.5625, 0.4362) and (0.5845, 0.4147) corresponding to the NPABSSm5, NPABSSm10 and NPABSSm15 glasses respectively. The CIE 1931 diagram for the Sm^{3+} doped borosilicate glasses is presented in **Fig. 10** and it is observed from the figure that the x, y coordinates are mostly located in the orange-red region of the CIE 1931 diagram. This indicates the fact that the reddish-orange emission can be achieved with the prepared Sm^{3+} doped borosilicate glasses.

Table 8 Emission peak wavelength (λ_p, nm), radiative transition probability (A, S^{-1}) effective line width ($\Delta\lambda_{eff}$, nm) and experimental branching ratio (β_R), experimental (τ_{exp}) and radiative (τ_{rad}) life times ((μs) and stimulated emission cross-section ($\sigma_p^E x10^{-22}$ cm^2) corresponding to the $^4G_{5/2}$ emission transitions of the NPABSSm glasses

Transition	Parameter	NPABSSm5	NPABSSm10	NPABSSm15
$^4G_{5/2}\rightarrow{}^6H_{5/2}$	λ_P	564	564	564
	$\Delta\lambda_{eff}$	12.69	11.9	14.13
	A	22.34	23.4	21.839
	σ_P^E $x10^{-22}$	0.863	0.964	0.756
	β_R (Exp)	0.094	0.055	0.086
	β_R (Cal)	0.148	0.149	0.162
	σ_P^E x $\Delta\lambda_{eff}x10^{-28}$	1.10	1.147	1.069
	σ_P^E x τ_R $x10^{-25}$	2.276	2.229	1.888
$^4G_{5/2}\rightarrow{}^6H_{7/2}$	λ_P	600	600	600
	$\Delta\lambda_{eff}$	14.98	14.5	15.98
	A	127.14	248.55	127.22
	σ_P^E	5.36	10.832	5.015
	β_R (Exp)	0.536	0.594	0.502
	β_R (Cal)	0.541	0.542	0.542
	σ_P^E x $\Delta\lambda_{eff}$	8.04	8.38	8.014
	σ_P^E x τ_R	17.864	25.054	12.531
$^4G_{5/2}\rightarrow{}^6H_{9/2}$	λ_P	648	648	648
	$\Delta\lambda_{eff}$	17.07	16.36	18.5
	A	51.63	98.05	44.76
	σ_P^E	2.58	3.2848	2.0478
	β_R (Exp)	0.218	0.234	0.177
	β_R (Cal)	0.268	0.281	0.274
	σ_P^E x $\Delta\lambda_{eff}$	4.404	5.373	3.788
	σ_P^E x τ_R	8.599	7.598	5.117
$^4G_{5/2}\rightarrow{}^6H_{11/2}$	λ_P	711	711	711
	$\Delta\lambda_{eff}$	18.91	18.3	19.91
	A	24.66	48.54	28.38
	σ_P^E	1.61	2.641	1.760
	β_R (Exp)	0.104	0.116	0.112
	β_R (Cal)	0.029	0.028	0.023
	σ_P^E x $\Delta\lambda_{eff}$	3.05	4.833	3.505
	σ_P^E x τ_R	5.366	6.109	4.398

3.9 CIE

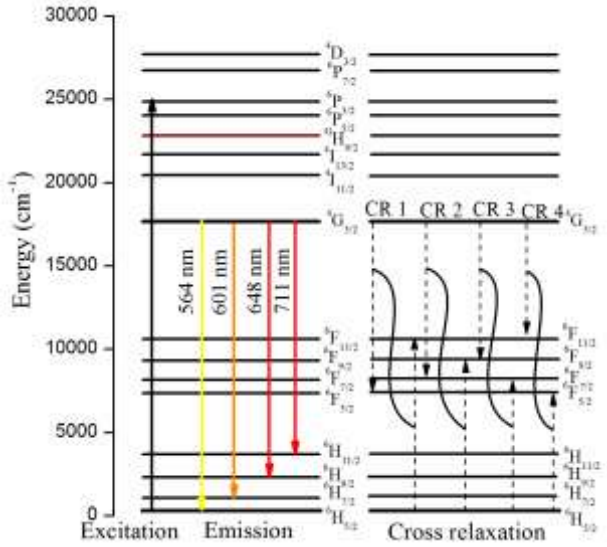

Fig. 9 Energy diagram of the Sm^{3+} ions in NPABS glasses

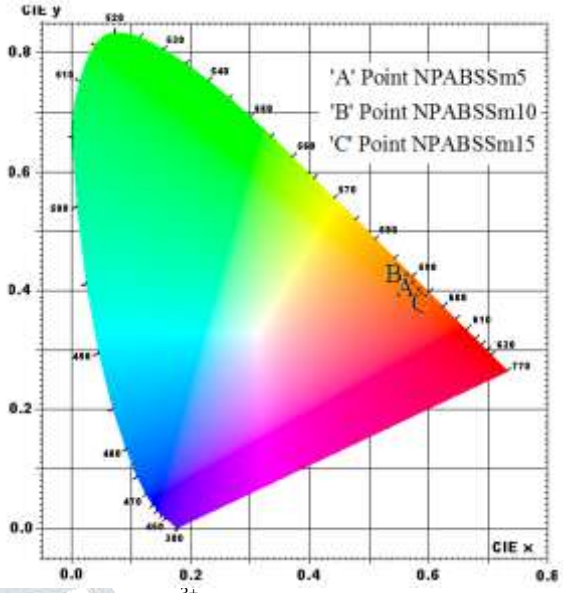

Fig. 10 CIE 1931diagram of the Sm^{3+} doped NPABS glasses

The CCT values of the prepared glasses are presented in **Table 9** along with the reported Sm^{3+} doped glasses [52]. It is observed that Sm^{3+} doped NPABS glasses emit reddish-orange light. It can be an alternative choice for the generation of new luminescence materials pertaining to reddish-orange emission and the present glasses can act as a promising candidate for reddish-orange light emitting diode applications under UV excitation.

Table 9 Sample code, chromaticity coordinates (x, y) and correlated color temperature (CCT) for various Sm^{3+} glass system

Sample code	Chromaticity coordinates		CCT(K)
	x	y	
NPABSSm5	0.5789	0.4202	1705
NPABSSm10	0.5625	0.4362	1826
NPABSSm15	0.5845	0.4147	1710

3.10 Fluorescence decay rates and quantum efficiencies

The decay rates for the $^4G_{5/2}$ level of Sm^{3+} ion in the present NPABS glasses have been obtained by exciting the sample. **Fig. 11** shows the decay curves for the $^4G_{5/2}$ level of Sm^{3+} doped NPABS glasses. It is noticed that the decay curve exhibit single exponential nature due to the energy transfer through cross-relaxation between the Sm^{3+} ions. The obtained experimental life time (τ_{exp}) values of the present glasses are found to be 1.974, 1.681 and 1.599 ms corresponding to the NPABSSm5, NPABSSm10 and NPABSSm15 glasses respectively [53, 54]. The effective decay time is evaluated using the following expression:

$$\tau_{exp} = \tau_{eff} = \frac{\int t\, I(t)dt}{\int I(t)dt} \qquad (15)$$

where I(t) is the emission intensity at time 't'. For the rare earth (RE) doped glasses, the experimental lifetime (τ_{exp}) is expressed using the expression [54]

$$\frac{1}{\tau_{exp}} = \frac{1}{\tau_{rad}} + +W_{MPR} + W_{ET} + W_{OH} + \cdots \qquad (16)$$

where τ_{rad} is the radiative lifetime determined through J-O theory, W_{MPR} is the multi phonon relaxation rate, W_{ET} is the rate of energy transfer and W_{OH} is the energy transfer rate between RE^{3+} ion and OH groups. The multi phonon relaxation in the prepared Sm^{3+} doped NPABS glass is very much suppressed, since the energy difference between $^4G_{5/2}$ level and the next lower level is 7000 cm^{-1} which is large enough to do so. The non-radiative decay rate is determined using the following expression:

$$W_{NR} = \frac{1}{\tau_{exp}} - \frac{1}{\tau_{rad}} \qquad (17)$$

The W_{NR} (s^{-1}) for the $^4G_{5/2}$ level is found to be 207, 177 and 225 S^{-1} for NPABSSm5, NPABSSm10 and NPABSSm15 glasses, respectively. The luminescence quantum efficiency (η) is defined as the ratio of the number of photons emitted to the number of photons absorbed. In the case of RE^{3+} ion incorporated systems, it is equal to the ratio of the measured lifetime to the predicted lifetime for the corresponding levels and is given by

$$\eta = \frac{\tau_{exp}}{\tau_{rad}} \text{ x } 100 \qquad (18)$$

The η values have been determined for the $^4G_{5/2}$ level of Sm^{3+} ions and are found to be 59, 73 and 64 % corresponding to the NPABSSm5, NPABSSm10 and NPABSSm15 glasses respectively. The non-exponential behavior due to the concentration quenching of Sm^{3+} ions arising from the ion-ion interaction usually due to the cross-relaxation process. The considerable value of the experimental radiative lifetime and the non-exponential behavior of the prepared glasses are mainly due to the energy transfer process among the neighboring Sm^{3+} ions. The cross-relaxation between the pair of Sm^{3+} ions and the migration of the excitation energy which in turn accelerate the decay by an energy transfer to the structural defects acting as energy sinks are the two probable reasons to have non-exponential behavior in the prepared glasses. The presence of OH-groups in the prepared glasses also play a dominant role in the quenching of excited state lifetime of Sm^{3+} ions [31]

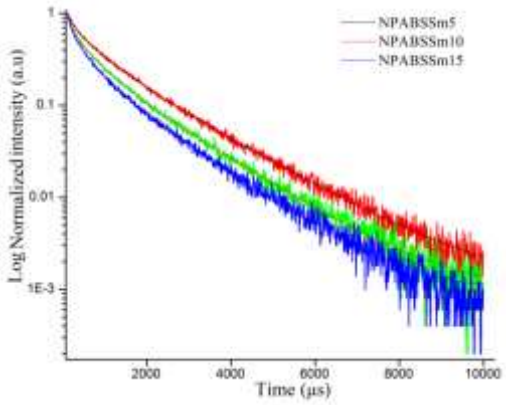

Fig. 11 Normalized decay curve of the $^4G_{5/2}$ level for Sm^{3+} ions in NPABS glasses

4. Conclusion

A series of Sm^{3+} ion doped sodium lead alumino borosilicate glasses are prepared by conventional melt quenching and pressing method. The amorphous nature is confirmed through the XRD spectral measurements. The presences of various stretching and bending vibrations of different borate and silicate networks have been identified from the FT-IR spectra. The ionic nature of the Sm^{3+} metal ligand bonding have been explored from the absorption spectral measurements and the ionicity decreases due to the decrease in Al_2O_3 content because of the fact the polarization of oxygen upon Sm^{3+} ions is higher. The band gap energy (E_g) values are found to decrease with the Sm^{3+} ion content due to the fall in non-bridging oxygens in the prepared glasses which shift the valence band in the downward direction. The lower Ω_2 intensity parameter values and the decreasing intensity ratio values prove that Sm^{3+} ions are located in a higher symmetrical environment and the same is further confirmed through the more ionic nature of the Sm-O bond. The $^4G_{5/2} \rightarrow {}^6H_{7/2}$ transition of the NPABSSm10 glass exhibit higher A, β_R, σ_p and gain bandwidth values and can be used as a potential active medium for the fabrication of visible solid state lasers, submarine communications and medical diagnostic applications. The x, y coordinates of the studied glasses passes through the reddish-orange region in the CIE 1931 diagram and is suitable for orange LEDs and visible laser applications. The decay profile of the studied glasses exhibit single exponential behavior for lower Sm^{3+} ion concentration and becomes non-exponential for higher Sm^{3+} ion content.

5. References

[1] Atul Khanna, Amanpreet Saini, Banghao Chen, Fernando Gonzalez, Carmen Pesquera, "Structural study of bismuth borosilicate, alumino borate and alumino borosilicate glasses by ^{11}B and ^{27}Al MAS NMR spectroscopy and thermal analysis", J. Non-Cryst. Solids 373 (2013) 34-41.

[2] F.H. ElBatal, M.S. Selim, S.Y. Marzouk, M.A. Azooz, "UV-vis absorption of the transition metal-doped SiO_2-B_2O_3-Na_2O glasses", Physica B 398 (2007) 126-134.

[3] Hongli Wen, Peter A. Tanner, "Optical properties of 3d transition metal ion-doped sodium borosilicate Glass", Journal of Alloys and Compounds 625 (2015) 328-335.

[4] Yasser B. Saddeek, Kamal A. Aly, Safaa A. Bashier, "Optical study of lead borosilicate glasses", Physica B 405 (2010) 2407-2412.

[5] R. Limbach, A.Winterstein-Beckmann, J. Dellith, D. Möncke, L. Wondraczek, "Plasticity, crack initiation and defect resistance in alkali-borosilicate glasses: From normal to anomalous behavior", J. Non-Cryst. Solids 417 (2015) 15-27.

[6] J. Santhan Kumar, J. Lakshmi Kumari, M. Subba Rao, Sandhya Cole, "EPR, optical and physical properties of chromium ions in CdO-SrO-B_2O_3-SiO_2 glasses", Opt. Mater. 35 (2013) 1320-1326.

[7] Ewan Maddrell, Stephanie Thornber, Neil C. Hyatt, "The influence of glass composition on crystalline phase stability in glass-ceramic waste forms", J. Nucl. Mater. 456 (2015) 461-466.

[8] E.O. Serqueira, N.O. Dantas, M.J.V. Bell, "Control of spectroscopic fluorescence parameters of Nd^{3+} ions as a function of concentration in a SiO_2-Na_2O-Al_2O_3-B_2O_3 glass system", Chem. Phys. Lett. 508 (2011) 125-129

[9] A. Rupesh Kumar, T.G.V.M. Rao, N. Veeraiah, M. Rami Reddy, "Fluorescence spectroscopic studies of Mn^{2+} ions in SrO-Al_2O_3-B_2O_3-SiO_2 glass system", Opt. Mater. 35 (2013) 402-406.

[10] N.C.A. deSousa, M.T. deAraujo, C. Jacinto, M.V.D. Vermelho, N.O. Dantas, C. C. Santos, I. Guedes, "The role of TiO_2 in the B_2O_3-Na_2O-PbO-Al_2O_3 glass system", J. Solid State Chem.184 (2011) 3062-3065.

[11] V. Madhuri, J. Santhan Kumar, M. Subba Rao, Sandhya Cole, "Investigations on spectral features of tungsten ions in sodium lead alumino borate glass system", J. Phys. Chem. Solids 78 (2015) 70-77.

[12] P. Pascuta, L. Pop, S. Rada, E. Culea, "The local structure of bismuth borate glasses doped with europium ions evidenced by FT-IR spectroscopy", J. Mater. Sci. Mater. Electron. 19 (2008) 424-428.

[13] S. Shanmuga Sundari, K. Marimuthu, M. Sivraman, S. Surendra Babu, "Composition dependent structural and optical properties of Sm^{3+} doped sodium borate and sodium fluoroborate glasses", J. Lumin. 130 (2010) 1313-1319.

[14] S. Selvi, K. Marimuthu, G. Muralidharan, "Structural and luminescence behavior of Sm^{3+} ions doped lead boro-telluro-phosphate glasses", J. Lumin. 159 (2015) 207-218.

[15] C. K. Jayasankar, V. Venkatramu, P. Babu, "High-pressure fluorescence study of Sm^{3+} doped borate and fluoroborate glasses", J. Appl. Phys. 97 (2005) 093523.

[16] Vineet Kumar Rai, Cid B. de Araujo., "Fluorescence intensity ratio technique for Sm^{3+} doped calibo glass, Spectrochim. Acta, Part A 69 (2008) 509-512.

[17] E. Malchukova, B. Boizot, G. Petite, D. Ghaleb, "Optical properties and valence state of Sm ions in alumino borosilicate glass under γ-irradiation", J. Non-Cryst. Solids 353 (2007) 2397-2402.

[18] C.K. Jayasankar, V.V. Ravi Kanth Kumar, "Judd-Ofelt intensity analysis and spectral studies of Pr(III) ions in alkali zinc borosulphate glasses", Mater. Chem. Phys. 46 (1996) 84-91.
[19] K. Linganna, Ch. Basavapoornima, C.K. Jayasankar, "Luminescence properties of Sm^{3+} doped fluorosilicate glasses", Optics Communications 344 (2015) 100-105.
[20] S. Arunkumar, K. Marimuthu., "Concentration effect of Sm^{3+} ions in B_2O_3-PbO-PbF_2-Bi_2O_3-ZnO glasses Structural and luminescence investigations", J. Alloys Compd. 565 (2013) 104-114.
[21] Fakhra Nawaz, Md. Rahim Sahar, S.K. Ghoshal, Asmahani Awang , Ishaq Ahmed, "Concentration dependent structural and spectroscopic properties of Sm^{3+}/Yb^{3+} co-doped sodium tellurite glass", Physica B 433 (2014) 89-95.
[22] Myoung Gyu Ha, Jae-Sun Jeong, Kyoung-Rim Han, Yangsoo Kim, Ho-Soon Yang, Euh Duck Jeong, K.S. Hong, "Characterizations and optical properties of Sm^{3+} doped Sr_2SiO_4 phosphors", Ceram. Int. 38 (2012) 5521-5526.
[23] Huajuan Deng, Ze Zhao, Jing Wang, Zhoufei Hei, Mengxue Li, Hyeon Mi Noh, Jung Hyun Jeong, Ruijin Yu, "Photoluminescence properties of a new orange-red emitting Sm^{3+} doped $Y_2Mo_4O_{15}$ phosphor", J. Solid State Chem. 228 (2015) 110-116.
[24] D. Ramachari, L. Rama Moorthy, C.K. Jayasankar, "Spectral investigations of Sm^{3+}-doped oxyfluorosilicate glasses", Mater. Res. Bull. 48 (2013) 3607-3613.
[25] E. Kaewnuam, H. J. Kim, C.K. Jayasankar, N. Chanthima, J. Kaewkhao, "The photoluminescence, optical and physical properties of Sm^{3+}-doped lithium yttrium borate glasses", Phys. Chem. Glasses: Eur. J. Glass sci. Technol. B 57 (2016) 85-89.
[26] K.K. Mahato, D.K. Rai, S.B. Rai, "Optical Studies of Sm^{3+} doped oxyfluoroborate glass", Solid State Commun. 108 (1998) 671-676.
[27] J. Anjaiah, C. Laxmikanth, N. Veeraiah, P. Kistaiah, "Infrared luminescence and thermoluminescence of lithium borate glasses doped with Sm^{3+} ions", Materials Science-Poland, 33 (2015) 144-151.
[28] A.G. Souza Filho, J. Mendes Filho, F.E.A. Melo, M.C.C. Custodio, R. Lebullenger, A.C. Hernandes, "Optical properties of Sm^{3+} doped lead fluoroborate glasses", J. Phys. Chem. Solids 61 (2000) 1535-1542.
[29] I. Pal, A. Agarwal, S. Sanghi, M.P. Aggarwal, "Investigation of spectroscopic properties, structure and luminescence spectra of Sm^{3+} doped zinc bismuth silicate glasses", Spectrochim. Acta, Part A: 101 (2013) 74-81.
[30] V. Venkatramu, P. Babu, C.K. Jayasankar, Th. Troster, W. Sievers, G. Wortmann, "Optical spectroscopy of Sm^{3+} ions in phosphate and fluorophosphate glasses", Opt. Mater. 29 (2007) 1429-1439.
[31] K. Maheshvaran, K. Linganna, K. Marimuthu, "Composition dependent structural and optical properties of Sm^{3+} doped boro-telluriteglasses ", J. Lumin. 131 (2011) 2746-2753.
[32] C.R. Kesavulu, C.K. Jayasankar, "Spectroscopic properties of Sm^{3+} ions in led fluorophosphate glasses", J. Lumin. 132 (2012) 2802-2809.
[33] Tran Ngoc, Vu Phi Tuyen, Phan Van Do, "Optical Properties of Sm^{3+} ions in Borate Glass", VNU Journal of Mathematics - Physics 30 (2014) 24-31.
[34] E. A. Davis, N. F. Mott, "Conduction in non-crystalline systems V. Conductivity, optical absorption and photoconductivity in amorphous semiconductors" Philos. Mag. 22 (1970) 903-922.
[35] G. Venkataiah, C.K. Jayasankar, K. Venkata Krishnaiah, P. Dharmaiah, N. Vijaya, "Concentration dependent luminescence properties of Sm^{3+}-ions in tellurite-tungsten- zirconium glasses", Opt. Mater. 40 (2015) 26-35.
[36] S. Babu, A. Balakrishna, D. Rajesh, Y.C. Ratnakaram, "Investigations on luminescence performance of Sm^{3+} ions activated in multi-component fluoro-phosphate glasses", Spectrochim. Acta, Part A: Molecular and Biomolecular Spectroscopy 122 (2014) 639-648.
[37] K. Swapna, Sk. Mahamuda , A. Srinivasa Rao, S. Shakya, T. Sasikala, D. Haranath, G. Vijaya Prakash, "Optical studies of Sm^{3+}ions doped Zinc Alumino Bismuth Borate glasses", Spectrochim. Acta, Part A: Molecular and Biomolecular Spectroscopy 125 (2014) 53-60.
[38] D. Umamaheswari, B.C. Jamalaiah, T. Sasikala, Il-Gon Kim, L. Rama Moorthy, "Photoluminescence properties of Sm^{3+}- doped SFB glasses for efficient visible lasers", J. Non-Cryst. Solids 358 (2012) 782-787.
[39] Y.N.Ch. Ravi Babu, P.Sree Ram Naik, K. Vijaya Kumar, N. RajeshKumar, A. Suresh Kumar,"Spectral investigations of Sm^{3+} doped lead bismuth magnesium borophosphate glasses", J. Quant. Spectrosc. Radiat. Transfer 13 (2012) 1669-1675.
[40] Y.C. Ratna karam, D. ThirupathiNaidu, R.P.S. Chakradhar, "Spectral studies of Sm^{3+} and Dy^{3+} doped lithiumcesiummixedalkali borate glasses", J. Non-Cryst. Solids 352 (2006) 3914-3922.
[41] S. Sailaja, C. Nageswara Raju, C. Adinarayana Reddy, Young-DahlJho, B.Deva Prasad Raju, B.Sudhakar Reddy, "Optical properties of Sm^{3+}-doped cadmium bismuth borate glasses", J. Mol. Struct. 1038 (2013) 29-34.
[42] Y.C. Ratnakarama, D. Thirupathi Naidu, A. Vijaya Kumar, N.O. Gopal, " Influence of mixed alkalies on absorption and emission properties of Sm^{3+} ions in borate glasses", Physica B 358 (2005) 296-307
[43] Hongli Liu, SongGuo, YuyingHao, HuaWang, BingsheXu, "Luminescent properties of Eu^{3+} and Sm^{3+} activated M_2SiO_4 (M = Ba, Sr and Ca) red-emitting phosphors for WLEDs", J. Lumin. 132 (2012) 2908-2912.
[44] H. Lin, X.Y. Wang, L. Lin, D.L. Yang, T.K. Xu, J.Y. Yu, E.Y.B. Pun, "Spectral parameters and visible fluorescence of Sm^{3+}in alkali-barium-bismuth-tellurite glass with high refractive index", J. Lumin. 116 (2006) 139-144.
[45] Zhiguo Xia, Daimei Chen, "Synthesis and Luminescence Properties of $BaMoO_4$: Sm^{3+} Phosphors", J. Am. Ceram. Soc. 93 (2010) 1397-1401.
[46] G. Lakshminarayana, Hucheng Yang, Yu Teng, Jianrong Qiu, "Spectral analysis of Pr^{3+}, $Sm^{3+}$and Dy^{3+}-doped transparent GeO_2-BaO-TiO_2 glass ceramics", J. Lumin. 129 (2009) 59-68.
[47] Phan Van Do, Vu Phi Tuyen, Vu Xuan Quang, Le Xuan Hung, Luong Duy Thanh, Tran Ngoc, Ngo Van Tam, Bui The Huy, "Investigation of spectroscopy and the dual Energy transfer mechanisms of Sm^{3+}-doped telluroborate glasses", Opt. Mater. 55 (2016) 62-67.
[48] C.K. Jayasankar, P. Babu, Optical properties of Sm^{3+} ions in lithium borate and lithium fluoroborate Glasses, J. Alloys Compd. 307 (2000) 82-95.

[49] R. Vijaya, V. Venkatramu, P. Babu, C.K. Jayasankar, U.R. Rodríguez-Mendoza, V. Lavin, "Spectroscopic properties of Sm^{3+} ions in phosphate and fluorophosphate Glasses", J. Non-Cryst. Solids 365 (2013) 85-92.
[50] I. Arul Rayappan, K. Selvaraju, K. Marimuthu, "Structural and luminescence investigations on Sm^{3+} doped sodium fluoroborate glasses containing alkali/alkaline earth metal oxides", Physica B 406 (2011) 548-555.
[51] Ki-Soo Lim, N. Vijaya, C.R. Kesavulu, C.K. Jayasankar, "Structural and luminescence properties of Sm^{3+} ions in zinc fluorophosphate glasses", Opt. Mater. 35 (2013) 1557-1563.
[52] M. Vijayakumar, K. Marimuthu, V. Sudarsan, "Concentration dependent spectroscopic behavior of Sm^{3+} doped leadfluoro-borophosphate glasses for laser and LED applications", J. Alloys Compd. 647 (2015) 209-220.
[53] Z. Mazurak, S. Bodyl, R. Lisiecki, J. Gabrys-Pisarska, M. Czaja, "Optical properties of Pr^{3+}, $Sm^{3+}$and Er^{3+} doped P_2O_5-CaO-SrO-BaO phosphate glass", Opt. Mater.32 (2010) 547-553.
[54] S. Krause, C. Pfau, M. Dyrba, P.T. Miclea, S. Schweizer, "On the role of the network modifier PbO in Sm^{3+}-doped borate glasses", J. Lumin. 15 (2014) 29-33.